

Research Article: New Research | Sensory and Motor Systems

Representation of natural contours by a neural population in monkey V4

<https://doi.org/10.1523/ENEURO.0445-23.2024>

Received: 25 October 2023
Revised: 18 February 2024
Accepted: 22 February 2024

Copyright © 2024 Machida et al.

This is an open-access article distributed under the terms of the [Creative Commons Attribution 4.0 International license](#), which permits unrestricted use, distribution and reproduction in any medium provided that the original work is properly attributed.

This Early Release article has been peer reviewed and accepted, but has not been through the composition and copyediting processes. The final version may differ slightly in style or formatting and will contain links to any extended data.

Alerts: Sign up at www.eneuro.org/alerts to receive customized email alerts when the fully formatted version of this article is published.

1 **Representation of natural contours by a neural population in monkey V4**

2

3

4 Itsuki Machida¹, Motofumi Shishikura¹, Yukako Yamane², and Ko Sakai¹

5

6 ¹ Department of Computer Science, University of Tsukuba, Tsukuba, Japan

7 ² Neural Computation Unit, Okinawa Institute of Science and Technology, Okinawa, Japan

eNeuro Accepted Manuscript

9 **Abstract**

10

11 The cortical visual area, V4, has been considered to code contours that contribute to the intermediate-
12 level representation of objects. The neural responses to the complex contour-features intrinsic to
13 natural contours are expected to clarify the essence of the representation. To approach the cortical
14 coding of natural contours, we investigated the simultaneous coding of multiple contour-features in
15 monkey (*Macaca fuscata*) V4 neurons and their population-level representation. A substantial number
16 of neurons showed significant tuning for two or more features such as curvature and closure,
17 indicating that a substantial number of V4 neurons simultaneously code multiple contour-features. A
18 large portion of the neurons responded vigorously to acutely curved contours that surrounded the
19 center of classical receptive field, suggesting that V4 neurons tend to code prominent features of
20 object contours. The analysis of mutual information (MI) between the neural responses and each
21 contour feature showed that the most neurons exhibited similar magnitudes for each type of MI,
22 indicating that many neurons showed the responses depended on multiple contour-features. We next
23 examined the population-level representation by using multi-dimensional scaling analysis. The neural
24 preferences to the multiple contour-features and that to natural stimuli compared to silhouette stimuli
25 increased along with the primary and secondary axes, respectively, indicating the contribution of the
26 multiple contour-features and surface textures in the population responses. Our analyses suggested that
27 V4 neurons simultaneously code multiple contour-features in natural images and represent contour
28 and surface properties in population.

30 **Significance Statement**

31 Contours of natural objects are often complex but the visual system extracts their features and
32 efficiently represent their shape. Neurons in the intermediate-level visual cortex, V4, play crucial roles
33 for the representation of natural contours. Analyzing the electrophysiological data, we found that V4
34 neurons simultaneously code multiple contour-features such as curvature, closure, and orientation, and
35 represent the prominent contours such as corners and bumps. For instance, a number of neurons
36 responded to acute curvatures that enclosed object extent. Mutual information and population analyses
37 showed that the responses of many neurons depend on multiple contour-features and represent the
38 contours and surfaces in population. A population of V4 neurons seems to encode complex but
39 prominent contours for the representation of natural objects.

40

eNeuro Accepted Manuscript

41 **1. Introduction**

42 Construction of meaningful objects from pixels of a retinal image is a crucial function of the visual
43 system. Along with the ventral pathway, from the early-level area (V1) to inferior temporal area (IT),
44 low-level image features are gradually transformed into the representation of objects. The information
45 for object properties, such as position, size and pose, increases along the ventral stream (Hong et al.,
46 2016). Human fMRI studies have also reported that the representation of multiple shape properties
47 such as curvature, medial axis, and silhouette, increased from posterior to anterior regions (Papale et
48 al., 2020). The shape information in early areas was transformed to category information in higher
49 areas (Zeman et al., 2020). A recent study using the adaptive methods reported that the estimated
50 optimal stimuli in the lower-level (V1/V2) areas included more monochrome contours than those in
51 V4, and the higher-level (IT) area included more higher-level visual attributes than V4 (Rose et al.,
52 2021). These studies indicate that the transformation from the local features to objects takes place
53 along the ventral pathway. The similar representations observed in Deep Convolutional Neural
54 Networks (CNNs) suggest the fundamental necessity of the gradual transformation (Zeman et al.,
55 2020).

56 Intermediate-level areas in the ventral pathway, such as V4, have been considered to play a
57 central role in the transformation with the construction of the mid-level representation of objects (e.g.,
58 (Rensink & Enns, 1995; Roe et al., 2012)). A number of studies have reported the preferences to
59 somewhat complex, multiple features in V4 neurons that appear to link the low-level features to an
60 object. For instance, V4 neurons were selective to curvatures wherein the responses were sensitive not
61 only to the magnitude of curvature but also to the direction of figure with respect to the contour (the
62 sign of curvature), indicating the object-based representation in V4 (Pasupathy & Connor, 1999, 2001;
63 Pasupathy et al., 2020). A pool of oriented Gaussian kernels was capable of estimating not only the
64 magnitude but also the sign of curvature (Mehrani & Tsotsos, 2023). Surface-based, object-centered
65 representation has also been reported to appear in the intermediate-level processing in a hierarchical
66 computation (Kubilius et al., 2014). The neural preferences to curvatures, orientations, and contours
67 need to be carefully discussed with the considerations on the construction of object-based
68 representation from multiple features.

69 Contours are the outlines of object shapes, and thus provide essential information for the
70 construction of the object-based representation (e.g., (Attneave, 1954; Elder et al., 2018)).
71 Psychophysical studies have reported the crucial role of complex contour-features including closure,
72 convexity and symmetry in the representation (Bertamini & Wagemans, 2013). Response priming has
73 been demonstrated for complex figural features such as closure and symmetry in addition to
74 traditionally-tested basic features such as color and shape (Schmidt & Schmidt, 2014). Recent studies
75 have also reported that closure is a prominent attribute not driven from good continuation and

76 proximity (Gerhardstein et al., 2012), and that closure and convexity are crucial for shape perception
77 (El-Shamayleh & Pasupathy, 2016; Schmidtman et al., 2015) and figure-ground segregation in
78 natural scenes (Burge et al., 2010). Although the importance of contour features has been discussed
79 with regard to the construction of the object-based representation, whether and how V4 neurons code
80 these contour features have not been clarified. It is crucial to examine the preference of V4 neurons to
81 various contour features that have been considered crucial but not systematically investigated, such as
82 closure and symmetry. We expect to observe the preferences to various contour features, including
83 orientation, curvature, closure, and symmetry, that might be essential and efficient for the construction
84 of the object-based representation. Similar to the joint coding of curvature and its orientation
85 (Pasupathy & Connor, 1999), we expect the simultaneous coding of multiple features, which appears
86 advantageous given the limited number of neurons.

87 The neural system seems to code complex contours by prominent features, as suitable for the
88 representation of natural objects (Attneave, 1954). Psychophysical studies have reported that curvature
89 extreme/maxima predominantly contributed to the perception of complex shapes (Habak et al., 2004).
90 A population analysis of the curvature selective neurons in V4 showed a bias toward acute curvatures
91 (Carlson et al., 2011). Other studies have also reported the responsiveness of V4 neurons to various
92 prominent features including radial and concentric shapes (David et al., 2006). Coding prominent
93 features is efficient from information aspect. Since the large portions of natural contours are linear or
94 smoothly curved and only small portions are the corners and acute curvatures, the indication of the
95 latter is more informative than the former (Timme & Lapish, 2018). The features of contours have
96 been discussed with geometrical features, such as orientation, curvature, closure, and symmetry,
97 however, what is fundamental and efficient for the construction of objects has not been fully clarified.
98 We expect that some prominent features that might be expressed by a combination of geometrical
99 features are suitable for the construction of objects and coded in V4 neurons. It could be difficult to
100 intuitively term the exact prominent features but the response dependence on multiple features might
101 provide important insights for the neural coding of complex contours.

102 Natural images have been known to evoke greater responses to a number of V4 neurons
103 compared to artificial gratings (David et al., 2006). The importance of population coding in V4 for
104 encoding complex contours has been reported (Kodama et al., 2022; Pasupathy & Connor, 2002;
105 Weiner & Ghose, 2015; Yamane et al., 2020b), however, what and how contour features and their
106 combinations are coded by neural population in V4 have not been clarified. The visual system might
107 have been evolved and optimized to natural environment. The responses to natural images are crucial
108 for understanding the essence of the cortical scheme that achieves efficient and optimal coding of
109 complex natural contours. In traditional visual neuroscience, well-controlled artificial stimuli have
110 been utilized for investigating the response dependence to a specific feature. However, in the
111 examination of the combinations of features, the control of artificial stimuli is impractical because of

112 the explosion in the number of combinations. Since natural contours include a variety of
113 combinations of multiple features with the probability inherent in the natural environment, the
114 analyses of the neural responses to natural contours appear crucial in the investigation of the
115 preferences to multiple contour features.

116 To approach the cortical coding of natural contour in the light of the construction of the
117 object-based representation, we examined the simultaneous coding of multiple features (closure,
118 curvature, symmetry, and orientation) and their population-level representation. We analyzed the spike
119 recordings from Macaque V4 while the animals were viewing a set of natural image patches whose
120 distributions of the four features were close to uniform and independent to each other. A substantial
121 number of neurons exhibited significant tuning for two or more features, indicating the simultaneous
122 coding of multiple contour-features. Many neurons responded vigorously to acutely curved contours
123 facing out of figure and surrounding the center of classical receptive field (CRF), suggesting the
124 coding of prominent features of contours. To quantitatively examine the dependence of neural
125 responses on multiple contour-features, we examined mutual information (MI) between the neural
126 responses and contour features and showed the similar degrees of dependence on multiple features.
127 Finally, we examined the population-level representation by using multi-dimensional scaling and
128 showed the contribution of contour-features to the representation. Our analyses suggested that V4
129 neurons simultaneously code multiple contour-features and represent contour properties in population.

130

131

132 **2. Methods**

133 **Electrophysiological data**

134 The electrophysiological experiments on two female macaque monkeys (*Macaca fuscata*) were
135 previously performed and reported elsewhere (Yamane et al., 2020b). Briefly, the surgery to attach the
136 head restraint and the recording chamber was performed under full anesthesia at least two weeks
137 before the recording. On the electrophysiological recording, the animals were anesthetized and
138 immobilized, and the stimuli were shown to the contralateral eye with appropriate contact lens by
139 LCD monitor 57 cm away from the animal. Neural activity of V4 neurons were collected by 32-
140 channel silicon probes arranged linearly or probes with eight shafts (Neuronexus Technologies, Ann
141 Arbor, MI, USA). Signals were amplified (x1000), filtered (0.5-8kHz) and recorded at a sampling rate
142 of 20kHz. The recorded signals were sorted offline by custom made sorting software (Tamura et al.,
143 2014). All animal experiments were performed in accordance with the guidelines of the National
144 Institute of Health (1996) and the Japan Neuroscience Society and were approved by the Osaka
145 University Animal Experiment Committee (certification no: FBS-13-003). The recorded data were
146 publicly available in the institutional archive (Yamane et al., 2020a)(<https://doi.org/10.18910/73784>).

147

148 **Stimuli**

149 In the electrophysiological experiments, natural image patches and their silhouette images were
150 presented to the animals. Refer to (Yamane et al., 2020b) and (Shishikura et al., 2023) for details. We
151 defined *contours* in natural image as those drawn by human participants (human marked contours
152 (HMC)) available in the Berkeley Segmentation Dataset
153 (<https://www2.eecs.berkeley.edu/Research/Projects/CS/vision/bsds/>). The drawn contours differed
154 across participants in details but those obtained by pooling ten participants appear to show reasonable
155 contours. Sub-regions (69×69 pixels) were extracted from the HMC so that the *contours passed*
156 *through the center* of the regions. As the distribution of contour shape is highly non-uniform in natural
157 scenes, the distributions of the degree of curvature, closure, and symmetry of contours were controlled
158 (uniformly selected from each range of these characteristics) (Sakai et al., 2015). Several examples of
159 natural contours are shown in Figure 1A-D, and all stimuli are shown in Extended Data Figure 1-1.
160 The mirror images were also presented; the original images were mirrored with respect to the tangent
161 of the contour passing through the patch center. The color of the mirror images was inverted so that
162 the polarity of the color contrast remained constant with respect to the central border. Including a
163 mirror-image variation of each patch, the total number of natural patches was 210. Psychophysical
164 experiments were performed to obtain the veridical figure-ground (FG) labels for all patches
165 (Shishikura et al., 2023; Yamane et al., 2020b). Silhouette stimuli were generated from the natural
166 patches by filling black and white to the figure and ground regions with respect to the contour that
167 passed through the stimulus center, respectively, or vice versa (filling white and black to the figure
168 and ground, respectively). The most stimuli did not include the intersection of contours, so that we
169 were able to fill the regions with black and white. In the two stimuli including the intersection, grey
170 was filled in the third region. To obscure the boundary between the patch and the grey background, we
171 attenuated the contrast towards the periphery with a Gaussian function. The stimulus images were
172 presented on a linearized display.

173

174 **Estimation of the CRF and visual response**

175 At the beginning of each recording session, we manually plotted the CRF center for multi-unit activity
176 and roughly estimated the CRF center. We ran a pre-examination session to estimate CRF size using
177 the grating patch pattern in different positions (square-wave grating patches with 12 variations of
178 frequency (3) and orientation (4)). The stimulus presentation positions and scaling were determined
179 using the results of this pre-examination session. Stimuli were scaled to cover the CRFs of the
180 recording units more than three times larger than the rough estimate of the CRF diameter, yielding a
181 stimulus size between 2.5 and 21 degrees. For the precise estimation of the CRF center and extent for

182 individual single unit, a set of grating patch pattern similar to the one explained above were presented
183 together with stimulus patches during main recording sessions. Grating patches (0.5 or 1 degree in
184 diameter) were shown in distinct positions (in a 5×5 grid, covering 3 to 12 degrees of visual angle).
185 Each patch was shown 10 times in pseudo-random order in each session. The neural responses were
186 approximated by a two-dimensional Gaussian for the estimation of the CRF. The CRF extent was
187 defined as a region within the 2SD of the Gaussian.

188

189 **The definition of contour features**

190 Four types of features, closure, curvature, symmetry, and orientation, were calculated from the
191 contours of the stimulus set. The values of the features were calculated based on the Cartesian
192 coordinates of the points along the human-drawn contour of the silhouette stimuli (refer to Figure 1A).
193 The calculated values were also applied to the corresponding natural stimuli. Only the contour points
194 within the extent of CRF ($< 2SD$) were subject to the calculation of features except symmetry.

195

196 *Closure*

197 The closure was quantified as how much the contour is closed *around the CRF center of a neuron*
198 (Sajda & Finkel, 1995). The closure was determined by extending 100 radial lines from the center of
199 the CRF with equal intervals, and counting the number of lines that collided with the stimulus contour.
200 The ratio of the collided radial lines was defined as closure. Note that only collision points within the
201 CRF extent were taken into account. The value of closure was given for every combination of a
202 stimulus and a neuron since the center of CRF depended on neurons, meaning that the closure value of
203 a single stimulus differed across neurons. The closure ranges between zero and one, with greater
204 values for more closed contours. Several example closures are shown in Figure 1A.

205

206 *Curvature*

207 Curvature was quantified as how much the stimulus contour *within the CRF extent* was curved in the
208 direction of figure. The curvature was defined as the inverse of the radius of the circle fitted to the
209 stimulus contour. Since the degree of curvature varies along a natural contour, we calculated multiple
210 local curvatures for a single stimulus. A schematic diagram of the curvature calculation is shown in
211 Extended Data Figure 1-2. All local curvatures were associated with the response of the neuron to the
212 stimulus in the later tuning analysis. Note that the value of curvature was given for every combination
213 of a stimulus and a neuron since the extent of CRF depends on neurons (refer to Figure 1-2A). We
214 used all local curvatures rather than the mean because taking a mean often distracted convex-concave

215 information and/or produced a bias towards dull (obtuse) curvature. It is important to keep local
216 curvatures for the analysis of V4 neurons since they show selectivity to the convex/concave-ness as
217 well as the degree of curvature, and respond to a part of an object contour if it matches with the
218 preference of the neuron irrespective of other parts (Pasupathy & Connor, 2001).

219 We started with setting local windows for the calculation of local curvatures (refer to Figure
220 1-2B). We set a variety of windows with various scales and locations and fitted a single circle to the
221 contour points within every window if it fell on to the CRF extent of the neuron. The window had four
222 scales: 0.1 ~ 1 of the stimuli. We slid the window in the vertical and horizontal directions for every 10
223 pixels on the stimulus and repeated the calculation unless the contour points within the window was
224 less than ten. By excluding circles with a large fitting error, only appropriate contours were utilized for
225 the following computation. The criteria for the fitting error differed among stimuli and were
226 determined as the 80-th percentile of the error distribution of that stimulus. The number of calculated
227 circles varied among the pairs of a stimulus and a neuron, with the maximum of 20.

228 The inverse of the radius of the fitted circle was taken for the estimation of curvature.
229 However, since this value was inversely proportional to the radius, this was not consistent with the
230 rate of change of the radius (actual curvature), specifically, absolute values of curvature with large
231 radii had values close to zero while absolute values of curvature with small radii had extremely large
232 values. In order to make the curvature as a value that varies at a constant rate of change, the following
233 function was used to flatten the curvature distribution.

$$234 \quad c' = \frac{2.0}{1 + e^{-ac}} - 1.0$$

235 c' is the value of the transformed curvature, c is the value before the transformation, and a is a constant
236 ($a = 20$) determined for the adjustment of the distribution by visual inspection. This function was
237 defined based on the squashing function of the previous research (Pasupathy & Connor, 2001).

238 Finally, the curvature, which we used in the tuning analysis, was given by adding convex-
239 concave information. The convex/concave-ness was given by a sign wherein convex and concave
240 curvatures with respect to the direction of the figure were multiplied by +1 and -1, respectively. The
241 figure-ground of the stimuli was determined by the psychological experiment in the previous study
242 (Sakai et al., 2015). Therefore, curvature ranges between -1 and 1, where 1 is a sharply-convex
243 contour with respect to the figure direction, 0 is a straight contour, and -1 is a sharply-concave
244 contour. Several example local curvatures are shown in Figure 1B.

245 Our aim was to examine the dependence of the neural responses on curvatures inherent in a
246 number of natural contours. We generated the histogram of all local curvatures within the natural
247 contours by decomposing the contour into one or multiple local curvatures and then pooling the local
248 curvatures across stimuli (given n local curvatures in m stimuli, the accumulative frequency is $n \times m$),

249 and weighted the local curvatures by the neural responses. In practice, we first generated a histogram
250 of local curvatures for a combination of a neuron and a stimulus (refer to the left panel of Figure 1-
251 2C). Next, by multiplying this histogram with the response of this neuron to this stimulus, we obtain
252 the response histogram of local curvatures for the combination of this neuron and stimulus (refer to the
253 right panel of Figure 1-2C). Finally, by adding these response histograms of the neuron across all
254 stimuli, we obtain the response histogram of local curvatures for this neuron. This histogram
255 represents the response dependence of the neuron to curvatures inherent in the set of natural stimuli.
256 Several example histograms are shown in Figure 1F. This method enabled the estimation of the
257 response dependence to curvature in natural contours. Specifically, high efficiency of this method in
258 the electrophysiological experiment was prominent; multiple curvatures were presented in a single
259 stimulus and the responses to many stimuli were pooled.

260

261 *Symmetry*

262 Symmetry was quantified as how much the contour was mirror symmetric with respect to a line
263 passing through the stimulus center (Sakai et al., 2015). Blurring the contour points by a Gaussian
264 with $SD = 2$ pixels, we calculated how many points were overlapped to each other when folded back
265 with respect to the line. The overlaps were calculated for a total of 24 radial lines with an equal
266 interval of 7.5 degrees, and the greatest overlap was used for symmetry. The values of symmetry were
267 normalized across all stimuli so that it ranges between 0 and 1. Several examples are shown in Figure
268 1C.

269

270 *Orientation*

271 Orientation was quantified as the tilt of the stimulus contour *within the CRF extent* of the neuron.
272 Since the local orientation varies along a natural contour, the mean of the multiple local-orientations
273 was defined as the value of orientation for a combination of a stimulus and a neuron. Here, we used
274 the mean value in order to focus on the rough tilt of the stimulus contour within the CRF and avoid
275 entangling interactions with curvatures that was defined based on multiple local curvatures.
276 Preliminary results based on the multiple local orientations did not show substantial differences in the
277 analyses. The local orientation was determined by selecting a line defined by two points separated by
278 five pixels along a contour and calculating the tilt of the line with respect to the horizontal. This
279 calculation was repeated for all pairs of points within the CRF. The orientation ranges between 0 and
280 180, and zero and 180 represent the horizontal. Several examples are shown in Figure 1D.

281

282 Estimation of tuning

283 We generated tuning maps and determined the significance of the tuning for every neuron and feature.
284 The tuning maps were the *histograms* with the mean number of spikes for each range of feature (e.g.,
285 Figure 1E, F, G, H), which were normalized by the maximum value within the map for the following
286 analysis. In closure, curvature, and orientation analyses which were calculated only within the CRFs,
287 we were unable to estimate feature values for neurons with smaller CRFs because a sufficient length
288 of a contour was not included in the CRF. The neurons with the missing feature-values were excluded
289 from the analyses of curvature and orientation. However, in the closure analysis, since most neurons
290 had missing values (especially at greater closure values), we did not exclude the neurons from the
291 analysis. The significance of tuning was determined by a permutation test of the curve fitting. We
292 compared the fitting errors of the original and shuffled maps, and determined as significant if the error
293 of the original was smaller than the bottom 1% of the errors of 1000 shuffled maps.

294

295 *The parameter analysis of the tuning curve*

296 The tuning maps were fitted by either Gaussian or cosine functions. The Gaussian function was used
297 for closure and symmetry analyses and defined as

$$298 \quad f(x) = a \exp\left(-\frac{(x-b)^2}{c^2}\right)$$

299 , where parameters a , b , and c were constrained by $0 \leq a \leq 1$, $0 \leq b \leq 1$, and $0 \leq c \leq 1$, respectively.

300 The strength of tuning (the degree of tuning) was defined by a/c . The goodness of fits were $0.14 \pm$
301 0.17 and 0.04 ± 0.06 (RMSE across the neurons in the normalized number of spikes; mean \pm SD) for
302 closure and symmetry, respectively. The width of tuning was 0.618 ± 0.23 and 0.638 ± 0.188 (half
303 width at half height; mean \pm SD).

304 The cosine function was used for curvature and orientation analyses. Because, many curvature
305 maps have a dent in the center (near 0), orientation maps have periodicity, and they achieved good fits
306 with the cosine function. The cosine function was defined as

$$307 \quad f(\theta) = a \cos(b\theta - c) + d \quad .$$

308 In the curvature analysis, c was constrained by $-1 \leq c \leq 1$. No constrain was given to a and d since the
309 fitting accuracy was greatly reduced when constrained. The parameter b was fixed to 1 for the sake of
310 simplicity. We did not optimize b for individual neurons (which could achieve better fits) since our
311 purpose was to examine the significance in response dependence and the optimal feature (curvature),
312 but not to examine detailed tuning properties. The goodness of fit was 0.036 ± 0.043 . The strength of
313 tuning was defined by a . In the orientation analysis, parameters were constrained by $0 \leq a \leq 1$, $b = 1$, 0

314 $\leq c \leq \pi$ (180°), and $0 \leq d \leq 1$. The goodness of fit was 0.12 ± 0.13 .

315

316 **Mutual information between the contour features and neural responses**

317 Mutual information (MI) in this analysis was defined as

$$318 \quad I(X; Y) = \sum_{x \in X, y \in Y} p(x, y) \log_2 \left(\frac{p(x, y)}{p(x)p(y)} \right)$$

319 , where $p(x)$ and $p(y)$ represent the probability distributions of the neural responses and contour
320 features, respectively. The number of bins for generating the probability distribution was determined
321 for each combination of a neuron and a feature by using Sturges' rule. The equation was defined as

$$322 \quad n_{bin} = 1 + \log(2n)$$

323 , where n_{bin} is the number of the bins and n is the number of the data. Since there were missing values
324 for closure, curvature, and orientation, the numbers of available data and bins differed depending on
325 the neurons. The significance of MI was determined with a permutation test ($p < 0.05$).

326 Wilcoxon rank-sum test was used for the comparison between the neurons that showed
327 significant tuning and those did not. Wilcoxon effect size was indicated by r (e.g.,
328 https://rpkg.s.datanovia.com/rstatix/reference/wilcox_effsize.html). One-sample permutation test was
329 used to examine the deviation of the greatest and least MIs from 0.25. The effect size (Cliff's delta)
330 was indicated by d .

331

332 **Natural-to-Silhouette preference**

333 We examined whether a neuron responded more strongly to natural or silhouette stimuli. This
334 preference (NS preference) was defined by the difference between the mean numbers of spikes to the
335 natural and silhouette stimuli as

$$336 \quad NS_{pref} = \frac{R_{Natural} - R_{Silhouette}}{R_{Natural} + R_{Silhouette}}$$

337 , where $R_{Natural}$ and $R_{Silhouette}$ represent the mean numbers of spikes for natural and silhouette
338 stimuli, respectively. NS preference takes positive and negative values when a neuron strongly
339 responds to natural and silhouette stimuli, respectively.

340

341 **Multi-dimensional scaling (MDS)**

342 We generated the response matrix that consisted of the normalized responses of each neuron to every
343 stimulus. The responses of a neuron to every stimulus were normalized by the maximum response of
344 the neuron across stimuli in order to focus on the similarities among response patterns. We performed
345 two types of MDS: MDS based on the responses to both natural and silhouette stimuli, and that based
346 only on the silhouette stimuli. The matlab function for nonmetric MDS, *mdscale*, was used with
347 Kruskal's normalized Stress-1 (the squared distance between the neurons) and a randomized initial
348 configuration. The metric MDS with *cmdscale* function resulted in the similar results. We examined
349 what the axes of the maps represent based on the tuning significance and NS preference. First, we
350 divided the MDS maps along the primary axis into five groups so that each group had the same
351 number of neurons. Within each group, we calculated the numbers of neurons that showed the tuning
352 significance to each contour-feature. Next, we examined the distributions of the significant neurons
353 with finer widths for the division (window) and moving average. Here, setting the division to contain
354 30 neurons, we slid the window over the MDS maps and counted the number of neurons with
355 significant tuning. The result was smoothed by the moving average so as to remove jaggies and
356 present the tendency with respect to the axis. The numbers of significant contour-features and the
357 optimal closures and curvatures were similarly smoothed. The optimal curvatures were normalized so
358 that they ranged between 0 and 1. The dependence of the secondary axis on the NS preference was
359 also similarly analyzed.

360

361 **3. Results**

362 Previous studies have clarified that V4 neurons respond to contour features including curvatures and
363 concentric shapes (Gallant et al., 1993; Pasupathy & Connor, 1999), however, how the neurons code
364 contour shapes included in natural images has not been clarified. To approach the cortical coding of
365 natural contour, we focused on four features, closure, curvature, symmetry, and orientation, and
366 examined how neurons in V4 code these contour features.

367

368 **Preferences to multiple contour-features**

369 To understand the contour coding in V4, we first quantified the four features of contour shapes and
370 examined the preferences of V4 neurons to the contour features. We extracted contours from local
371 natural images, and quantified the contour features, *i.e.*, closure, curvature, symmetry, and orientation.
372 Closure represents how much the contour was closed around the CRF center of a neuron (Sajda &
373 Finkel, 1995). We defined closure as the ratio of the radial lines that were originated from the CRF
374 center and collided with the contour. The closure ranges between 0 and 1 ([0, 1]) with a few examples
375 shown in Figure 1A. Curvature represents how much the contour was curved with respect to the

376 direction of figure, and was defined by the inverse of the radius of the circle that was fitted to the
377 contour. The curvature ranges from -1 (concave) to $+1$ (convex) ($[-1, 1]$), with an identical magnitude
378 indicating the identical contour but the opposite sign indicating the other direction of figure. A few
379 examples are shown in Figure 1B. Since a curvature often varies along a contour in natural images, we
380 computed multiple curvatures within the CRF extent and used these values as curvature for a
381 combination of a stimulus and a neuron. Symmetry represents how much the contour was mirror
382 symmetric, and was defined by the ratio of pixels that overlapped with the corresponding pixel in the
383 other half with respect to the line passing through the stimulus center (Sakai et al., 2015). A few
384 examples are shown in Figure 1C. Since symmetry is considered as a global factor, we computed a
385 single value of symmetry for each stimulus ($[0, 1]$) without considering the location of the CRF center.
386 Orientation represents how much the contour was tilted, and was defined by the mean orientation
387 along the contour, so that a single value ($[0, 180]$) was computed for each stimulus. A few examples
388 are shown in Figure 1D. Detailed definitions of the four contour-features were given in Methods. The
389 stimuli used in the experiments had been selected to have wide and quasi-uniform distributions of
390 convexity, closure, symmetry, and orientation (Sakai et al., 2015)(refer to Figure 2B) without
391 dependence to each other so that the following analyses were performed with reasonable or no
392 compensation for the biases due to the distribution and dependence of the features. To illustrate the
393 independence of factors, the correlation between the closure and curvature is presented in Extended
394 Data Figure 1-3 together with example stimuli that could be considered weird such as “strongly curved
395 but not closed contours”.

396 We examined the preferences and tuning to the four contour-features of the recorded neurons.
397 The recorded data are available in the institutional archive (Yamane et al., 2020a:
398 <https://doi.org/10.18910/73784>). Tuning maps for every neuron were generated, which were
399 histograms of mean spike-counts in response to the contour features. Example tuning maps of a few
400 neurons were shown in Figure 1E-H, together with example time courses of ten neurons that were
401 randomly chosen from those with significant tuning (Figure 1I). Response variability appears different
402 across neurons, however, the variability (SD) across trials for individual stimuli was not related to the
403 strength of tuning (the mean SD across stimuli versus the tuning strength for individual neurons, $R^2 =$
404 0.090 and 0.079 for closure and curvature, respectively). The tuning maps were fitted with either a
405 Gaussian or a cosine function, and their statistical significance were tested with permutation tests
406 (refer to Methods for details). A number of neurons exhibited significant tuning for the contour
407 features (closure: 16.2% (118/728), curvature: 20.4% (99/486), symmetry: 4.7% (57/1217),
408 orientation: 16.5% (92/558)). The ratio of neurons with significant tuning was similar to or somewhat
409 smaller than the previous studies (Gallant et al., 1993; Pasupathy & Connor, 1999). Since we analyzed
410 all neurons with visual responses that were recorded with multiple micro-electrodes, a population
411 might include neurons with various preferences and/or low responses and result in a smaller number of

412 significant neurons. Furthermore, our fitting method was not as precise as the previous studies, which
413 might have resulted in slightly smaller ratios. The significant tuning for curvature and orientation was
414 consistent with the previous studies (Pasupathy & Connor, 1999). The tuning for closure and
415 symmetry suggests that a portion of V4 neurons code these Gestalt factors. The ratio of neurons with
416 significant tuning to closure was similar to those to curvature and orientation, which appears to be the
417 first quantitative report and provides solid support for coding multiple features. A more detailed
418 analysis is given in the next section.

419 We also analyzed the distribution of the optimal features of the neurons (Figure 2). The
420 optimal feature was estimated from the peak of the tuning function (e.g., closure = x , if the tuning
421 function peaks at x) as illustrated in Figure 2A. The distribution of the optimal closure (Figure 2C, the
422 top panel) was normalized by the probability density of the distribution of closure across stimuli
423 (Figure 2B, the top panel) since the number of stimuli that included a particular closure varied. The
424 normalized optimal closure roughly increases towards the greater closure (Figure 2D, the top panel).
425 The distribution of the optimal curvatures shows a strong bias towards acute curvatures (around -1
426 and $+1$; Figure 2D, the second panel), which agree with the previous report (Pasupathy & Connor,
427 2002). The distributions of the optimal symmetry and orientation appear relatively uniform in
428 comparison with closure and curvature (Figure 2D, the third and fourth panels, respectively). Uneven
429 distributions of the optimal curvature and closure are insightful in the investigation of the functional
430 roles of contour coding in V4. The biases toward closed contours and acute curvatures might indicate
431 that V4 neurons tend to code prominent and characteristic features of object contours. These results
432 indicated that each contour feature (closure, curvature, symmetry, and orientation) was coded by these
433 V4 neurons. Coding these features by a local population of neurons appears advantageous in the
434 construction of object-based representation that needs to combine multiple features. We next
435 examined the simultaneous coding of multiple contour-features by these individual neurons with a
436 specific interest in coding curvature and closure.

437

438 **Simultaneous tuning across multiple contour-features --- curvature and closure**

439 We investigated the coding of multiple contour-features by individual neurons. First, we analyzed
440 whether the neurons simultaneously code the multiple features. Among the neurons that all four
441 features were examined (refer to Methods for details), approximately a half of neurons (178/330)
442 exhibited significant tuning for at least one feature, and 33% (59/178) of them showed significant
443 tuning for multiple (two or more) features (Figure 3A). This result indicates that a substantial number
444 of V4 neurons simultaneously code multiple contour-features. Among 59 neurons that showed
445 multiple tuning, 49% (29/59) exhibited significant tuning to closure and curvature, 32% (19/59) to
446 closure and orientation, and 19% (11/59) to curvature and orientation. All combinations including

447 those with a smaller number of neurons were shown in Extended Data Figure 3-1.

448 We next examined the neural coding of closure and curvature that appeared crucial factors for
449 encoding contours. Since closure and curvature are not geometrically independent in general, we
450 examined the independence of tuning between the two features. Specifically, we examined whether
451 neurons tuned to acute curvatures were also tuned to closed contours. The degree of tuning across the
452 neurons that exhibited significance to closure and/or curvature ($n = 170$; including neurons whose
453 orientation tuning was not examined) showed a wide distribution without substantial correlation
454 (Figure 3B, $R^2 = 0.15$), indicating the existence of neurons tuned to closure in addition to those tuned
455 to curvature. Among these 170 neurons, 42% (71/170) of neurons exhibited tuning only to closure,
456 36% (62/170) only to curvature, and 22% (37/170) to the both, indicating similar contribution of the
457 two features to the contour representation. These results are consistent with the fact that Gestalt
458 psychology described closedness as an individual factor in addition to convexity (*i.e.*, curvature in the
459 present paper).

460 An important role of V4 is to form the intermediate-level representation of object shape.
461 Examination of the neural tuning to the combinations of contour features is crucial for understanding
462 what the neurons essentially code about object shape. Focusing on the neurons tuned to closure and/or
463 curvature ($n = 170$), we examined the cross-tuning of the closure and curvature (Figure 3C). To
464 compensate the bias due to unequal numbers of stimuli for every closure and curvature value (refer to
465 Figure 2B), we normalized the cross-tuning distribution based on the probability density of the number
466 of stimuli (Figure 3D). Note that the correlation between closure and curvature across stimuli was
467 negligible ($R^2 < 0.001$, Figure 3D) since we designed the stimulus set to assure the independence
468 (refer also to (Sakai et al., 2015)). The normalized cross-tuning exhibits a strong bias towards a greater
469 curvature and closure (Figure 3E). The same tendency is observed for a subset of the neurons that
470 were tuned to both closure and curvature ($n = 37$; Figure 3F-H). The bias towards acute curvature is
471 consistent with the previous reports (Pasupathy & Connor, 2002). An acute curve facing out of figure
472 and surrounding the CRF composes a convex figure-region that is common across the most of objects.
473 Therefore, this response tendency supports the construction of objects based on the simultaneous
474 coding of multiple features. The distribution of stimuli was biased toward approximately closure = 0.4
475 and curvature = 0 (Figure 3D&G), indicating that a relatively large number of contours were linear,
476 which seems to be expected in local natural images. However, our analysis showed that a large
477 number of neurons responded vigorously to infrequent features (acutely curved contours). Focusing on
478 a few but prominent feature is efficient from the aspect of information theory. Our results suggested
479 that V4 neurons tend to efficiently code prominent and characteristic features of object contours.

480

481 **Response dependence on multiple contour-features --- mutual information between features and**

482 **responses**

483 To quantitatively examine the response dependence on multiple contour-features, we examined mutual
484 information (MI) between the neural responses and contour features. If neurons similarly code
485 multiple features, rather than dominantly code a single feature, each feature would share a similar
486 amount of MI. Although the tuning analysis in the previous sections showed the preferences to certain
487 features in individual neurons, the analysis was based on models (fitted by a Gaussian or Cosine
488 function) and often did not reach significance even though the feature dependence was observable.
489 The model-based approach is insufficient for the quantitative comparison of the response dependence
490 on multiple features. MI are advantageous in the quantitative examination of the relation between the
491 responses and features because MI are independent of models such as tuning functions and
492 correlations (e.g.(Cover & Thomas, 2006)). We computed MI for the four contour features such as
493 closure, curvature, symmetry and orientation (MI_{clos} , MI_{curv} , MI_{symm} , MI_{orien} , respectively). MI_{feature}
494 was defined as

495

$$496 \quad MI_{\text{feature}}(X;Y) = \sum_{x \in X, y \in Y} p(x,y) \log_2 \left(\frac{p(x,y)}{p(x)p(y)} \right) \quad (1)$$

497

498 , where $p(x)$ and $p(y)$ represent the probability distributions of the neural responses and contour
499 features, respectively. Since the amount of MI depended on the number of spikes when the response
500 was weak (<15 spikes; refer to Extended Data Figure 4-1A-D), the weak neural responses were
501 excluded from the following analyses, which resulted in 100, 97, 146, and 100 neurons for closure,
502 curvature, symmetry, and orientation, respectively, being examined. The analyses without the
503 exclusion of weak responses did not alter the results (refer to Extended Data Figure 4-1).

504 The computed MI for individual neurons showed wide distributions that ranged between 0 and
505 0.15 bits (Figure 4A-D). The ratios of neurons with significant MI were 81% (81/100), 65% (63/97),
506 60% (87/146), and 77% (77/100) for closure, curvature, symmetry, and orientation, respectively
507 (permutation test, $p < 0.05$). The ratios of neurons with tuning whose significance was tested by the
508 permutation (refer to Methods) were 43% (43/100), 31% (30/97), 3% (5/146), and 43% (43/100) for
509 closure, curvature, symmetry, and orientation, respectively. The ratios of neurons with significant MI
510 were substantially greater than those with significant tuning; the former was approximately twice the
511 latter (symmetry: x17). Among the neurons with significant MI, the ratios of neurons with significant
512 tuning were 43% (35/81), 37% (23/63), 5% (4/87), and 52% (40/77) for closure, curvature, symmetry,
513 and orientation, respectively. These results indicate that a large number of V4 neurons exhibit contour
514 feature-dependent responses while their tuning often did not reach significance. If the neurons

515 responded to multiple features, their tuning for individual features might tend not to be significant
516 because of interaction while their responses would show the dependence on the features. This
517 tendency is consistent with the present result. Other possibilities include plural optimal features in
518 tuning; if this was the case, the neuron might show significance in MI but not in tuning. The tendency
519 of a greater number of MI-significant neurons would also be observed if the sensitivity for MI was
520 greater than that for tuning (*i.e.*, tuning tend not to be significant compared to MI). If this was the case,
521 the neurons with significant tuning might be expected to show greater MI. This tendency was slightly
522 observed in MI_{clos} , MI_{curv} , and MI_{orien} but was marginally or not significant (MI_{clos} , $p = 0.042$, $r = 0.19$;
523 MI_{curv} , $p = 0.94$, $r = 0.007$; MI_{symm} , $p = 0.19$, $r = 0.14$; MI_{orien} , $p = 0.19$, $r = 0.12$; Wilcoxon rank-sum
524 test; Figure 4A-D). These results also support that the neurons code multiple contour-features.

525 We next examined how individual neurons code the contour-features, specifically, whether
526 neurons dominantly code a single feature or similarly code multiple features. If a neuron coded a
527 single feature, the corresponding MI would dominate the others. Whereas if a neuron coded multiple
528 features, multiple MI would share similar magnitudes. The most neurons exhibited four types of MI
529 with similar magnitudes and few showed single dominant MI (Figure 4E), indicating that a large
530 number of neurons showed the responses dependent on multiple contour-features. If the stimulus
531 features were not independent to each other (e.g., more-closed contours tend to have more-acute
532 curvatures), we would need to compensate the dependence in this analysis. However, our stimulus set
533 was designed to satisfy the independence (correlation coefficient $R < 0.1$, $p > 0.37$), and thus no
534 compensation is necessary. For further confirmation, we examined the ratio of the greatest and least
535 MI with respect to the sum of the four types of MI (Figure 4F&G). The ratios for the greatest and least
536 were 0.33 and 0.20, respectively, indicating only slight biases (from 0.25) toward a single feature
537 (permutation test; $p < 0.001$, $d > 0.69$). These results support that a large number of V4 neurons code
538 multiple contour-features with similar but slightly biased weights among the features. Previous studies
539 have shown the responsiveness of V4 neurons to a number of features (e.g., (Gallant et al., 1993)). The
540 present study showed the response dependence to the four features that can be geometrically defined.
541 It might be plausible that V4 neurons show the response dependence on other features. It might also be
542 possible that the optimal contour-features of these neurons are more abstract than easily definable
543 simple geometric features.

544

545 **Population coding of contour shape and surface texture**

546 We next examined the population-level representation of contour shape by using multi-dimensional
547 scaling (MDS) analysis. Decoding population activities in response to contour features by using
548 machine learning methods could be straightforward to reveal the representation. However, decoding of
549 the combinations of multiple continuous values (contour features) is challenging, and furthermore, a

550 large number of data is required for learning. We have chosen to apply MDS which has been shown to
551 be simple and meaningful even with a relatively small number of data. V4 neurons seems to code
552 relatively complex contours that are defined by a combination of multiple features rather than a single
553 feature. We expect to observe a combination of features in the population-level representation.
554 Specifically, an axis of MDS is expected to represent the combination of contour features. The
555 response matrix for each neuron was comprised of the normalized spike-responses to the presented
556 stimuli, and the MDS map was generated from the similarities across the response matrices of the
557 neurons (refer to Methods and Materials for details). The neurons subject to the analyses were
558 identical to those used for the tuning analysis (n=330). We employed the two-dimensional (2D) MDS
559 map for the following analysis since the stress was substantially small with 2D (Extended Data Figure
560 5-1).

561 A wide distribution of neurons was observed on the 2D MDS map (Figure 5A, the top panel).
562 We explored a factor that contributed to the primary axis, including the contour features, their
563 combinations, luminance contrast, and FG configuration. We observed the correspondence of the axis
564 with the number of significantly tuned contour-features. First, the neurons were divided into groups
565 along with the primary axis, and the ratios of neurons with significant tuning were calculated for each
566 group. Specifically, we computed the windowed average with a small division and a moving
567 increment (see Methods for details; Figure 5A, the middle panel). The ratios of the neurons with
568 significant tuning increased along with the axis for all features except symmetry. Next, we computed
569 for each division of neurons the mean number of significant contour-features that indicates the degree
570 of multiple-tuning. The computed numbers were similarly smoothed and shown in the bottom panel of
571 Figure 5A. The number of significant features increased along with the axis.

572 The above analysis included both natural and silhouette stimuli. The responses to natural
573 stimuli included the responses to surface properties such as texture and color in addition to contour
574 features. To focus on the contour features, we excluded the responses to natural stimuli and performed
575 the identical analysis only with the responses to silhouette stimuli (Figure 5B). The obtained MDS
576 map exhibited the similar tendency that the number of encoded features increased along with the
577 primary axis with a substantially greater degree (the bottom panel). To quantitatively examine this
578 tendency, we applied a linear regression model with the number of significant features as the
579 dependent variable. The coefficient of determination (R^2) was 0.21 ($R = 0.46$, $p < 0.001$). This result
580 indicates that the number of encoded contour-features contributes to the primary axis. Single features
581 such as closure and curvature did not show the correspondence to the axis (the bottom panel). These
582 results suggest that the degree of multiple tuning substantially contributes to the response patterns of
583 neurons. The neurons tuned to multiple features might be capable of reliably detecting specific
584 contours, such as prominent contours consisting of an acutely curved contour surrounding a figural
585 region, while those tuned to a single feature tend to respond to relatively simple contours (for more

586 discussion, refer to Discussion section and Extended Data Figure 5-2). The result of MDS can be
587 considered as that neurons were categorized by the degree of complexity in their preference to contour
588 features, *i.e.*, how complex is the contour feature a neuron is capable of detecting. Although it could
589 have been also expected that a certain contour-feature such as closure and curvature corresponded to
590 the axis, the result showed that the number of encoded features, rather than a single geometrical
591 feature, corresponded to the axis (the bottom panel of Figure 5A&B). These results suggest that V4
592 neurons code a variety of contour features from simple bars to complex features in population. The
593 results also imply that V4 neurons respond not only to geometrical features that can be easily
594 parameterized but also to unknown prominent (relatively complex) features that greatly contribute to
595 the representation of natural objects.

596 We next explored a factor that contributed to the secondary axis, and observed the
597 correspondence of the axis with the preference to natural stimuli compared to silhouette stimuli (NS
598 preference). The NS preference was defined by the difference between the responses to natural and
599 silhouette stimuli (refer to Methods for details). The degree of NS preference roughly increased along
600 with the secondary axis (Figure 5C). A linear regression model with the NS preference as the
601 dependent variable showed a good fit with $R^2 = 0.28$ ($R = 0.53$, $p < 0.001$). Neurons with a greater NS
602 preference represent surface properties probably in addition to contour shapes, and those with a lesser
603 NS preference represent only contour shapes. Therefore, the degree of coding surface properties
604 appears to substantially contribute to the response patterns of neurons. These results suggest that V4
605 neurons encode surface properties and contour features by population. The previous studies have
606 reported the preference of V4 neuron to surface textures (Arcizet et al., 2008; Okazawa et al., 2015)
607 and also the independent/joint coding of textures and contour shapes (Kim et al., 2019; Pasupathy et
608 al., 2019). The result of the present analysis is consistent with these previous reports in that encoding
609 surface properties is crucial in addition to encoding contour features. We aimed to investigate the
610 representation of natural contours, however, the MDS analysis indicated the strong influence of
611 surface properties. The simultaneous examination of contour features and surface properties would
612 provide clues for further understanding of the representation in V4.

613

614 **4. Discussion**

615 We investigated the simultaneous coding of multiple contour-features inherent in natural images in
616 monkey V4 neurons and their population-level representation. The neurons showed significant tuning
617 to contour features including closure, curvature, and symmetry. A substantial number of neurons
618 showed significant tuning for two or more features. The most neurons exhibited the similar
619 magnitudes in MI for multiple features. These results indicate that a substantial number of V4 neurons
620 simultaneously code multiple contour-features. The MDS analyses showed the contribution of contour

621 features and surface properties to the population responses. These results suggest that V4 neurons
622 simultaneously code multiple contour-features and represent contour and surface properties in
623 population.

624 The distribution of the contour features across stimuli and that of the optimal features across
625 neurons showed the opposite patterns, which was specifically noticeable in closure and curvature,
626 indicating that the neurons responsive to sporadic features outnumbered those responsive to abundant
627 features. This tendency appears to be efficient in contour coding. For instance, the distribution of
628 curvature showed that a large portion of contours were close to straight lines, whereas straight
629 contours might not provide prominent information in shape coding. In contrast, acutely curved
630 contours which were rare in the distribution appear to provide more information and could be crucial
631 for the identification of shape. It might be important to focus on rare features in shape coding and
632 efficient to dispense more resources to rare features (e.g., (Timme & Lapish, 2018)). Given the limited
633 computational resources in the cortex and the necessity for efficient coding therein, the distribution of
634 the neural preferences to the contour features might reflect a fundamental aspect of cortical encoding.

635 Although a substantial number of natural objects are symmetric and the solid perceptual
636 representation of symmetry has been reported (e.g., (Sakai et al., 2021; Sharman & Gheorghiu, 2018)),
637 only a fraction of V4 neurons showed significant tuning to symmetry in the present experiment. The
638 limited spatial extent of the receptive field might account for this discrepancy. Since the extents of
639 CRFs are limited in V4 neurons, symmetric contour might not fall onto the CRF, and thus the neuron
640 is not capable of detecting symmetry even if it preferred symmetry. In fact, the CRF extents of a large
641 majority of the neurons did not cover the symmetric contour presented in the experiment.
642 Furthermore, even when the symmetric contour fell onto the CRF, the symmetry axis might often fell
643 outside the central region of the CRF. In this case, the detection of symmetry might be challenging
644 unless solid invariance to translation and rotation were present. These tendencies appear to limit the
645 present experiment in examining the preference to symmetry. It is also possible that V4 neurons might
646 not code symmetry. Neurons in higher cortical areas, such as IT, have larger receptive fields than V4,
647 and may be suitable for the detection of symmetry. A strong influence via feedback from the higher
648 areas might account for our observation that a few neurons showed significant tuning to symmetry.

649 The analysis of MI showed that a large number of neurons exhibited similar magnitudes for
650 the four types of MI, suggesting that the four contour features contribute similarly to the neural
651 responses. To quantify whether many neurons share the similar degrees of MI among the features, we
652 estimated the variance among the four types of MI for each neuron and computed the mean across the
653 neurons. The mean variance was small (0.0037), indicating that the responses of a large number of
654 neurons were similarly influenced by multiple contour-features. This result might be plausible. Since
655 V4 is the intermediate-level stage along the pathway from the detection of local contours to the

656 recognition of an object (e.g., (Yamane et al., 2008)), V4 neurons are expected to code object features
657 such as relatively complex shape (e.g., (Kubilius et al., 2014)). Each of four contour features, closure,
658 curvature, symmetry, or orientation, was one of parameters that could define shape. A combination of
659 the features seems suitable for the representation of relatively complex contour-patterns. V4 neurons
660 are expected to code relatively complex contour-patterns that are defined by a combination of multiple
661 parameters rather than to code a single feature of contours. The similar degrees of the four types of MI
662 support this expectation. The estimation of optimal contour-patterns would help understand the coding
663 scheme in V4. A reverse correlation method that was recently applied to estimate the effective spatial
664 extent of figure in V4 neurons (Kimura et al., 2022) might be applicable to the estimation of the
665 optimal contour features.

666 The MDS analysis showed the contribution of the number of significant contour-features to
667 the population representation. This result led us to expect V4 neurons for coding complex, prominent
668 contours as well as simple contours. However, we have not been able to present the optimal stimuli for
669 the neurons. Example stimuli that evoked strong responses to a few typical neurons are shown in
670 Extended Data Figure 5-2. It is expected to observe more complex contours in the stimuli that evoked
671 strong responses to the neurons with multiple tuning (pink neurons in Figure 5A&B) compared to
672 those with a single significant feature (red neurons). A reverse correlation technique might be
673 expected to reveal the optimal stimuli of the neurons, but it has not been successful because of the
674 spatial invariance of the preferences to contour features and the lack of a sufficient number of data.

675 The present MDS analysis focused on the preferences to the contour features and surface
676 properties. We have also carried out the analyses on the contribution of other features, such as
677 curvature, orientation, luminance contrast and FG, to which V4 neurons were reported to show
678 preference. However, these features did not show the contribution to the coordinates derived by the
679 MDS. These results suggest that these individual features were less effective than the combinations of
680 features and the surface properties in population coding. Furthermore, the results imply that V4
681 neurons code unknown prominent features that greatly contribute to the representation of objects and
682 are abundantly inherent in natural images. This result supports the importance of natural images for
683 investigating the representation of visual cortices and suggests the direction of future research. It
684 should be noted that the present analysis only examined the contribution of the four contour features
685 and surface properties to the primary and secondary coordinates in two-dimensional MDS. Other
686 features might be veiled in higher coordinates. Other methods, such as non-linear principle component
687 analysis (Okazawa et al., 2021) and representational similarity analysis (Kriegeskorte et al., 2008),
688 might be capable of unveiling other features, and thus advance the investigation on population coding
689 in V4.

690 We sought to investigate the intermediate-level representation in the visual cortex V4, with

691 specific interests on the formation/construction of the representation of objects. The present results on
692 the simultaneous coding of multiple contour features would provide insights in the coding of shared
693 features and feature binding (e.g., (Roelfsema, 2023; Willeke et al., 2023)). The recent investigations
694 on machine learning and CNNs proposed the concept of disentangling representation (Dado et al.,
695 2023; Klindt et al., 2023). In classification problems, the representation of exact shape/object might
696 not be necessary and other abstract features that are suitable for the representation of specific attributes
697 (such as facial expression and identity) might be desired (disentangling representation). This
698 representation might also be considered as an outcome of reasonable feature binding. Our first result
699 of the simultaneous coding of multiple contour-features is consistent with the concept of coding
700 multiple features of objects. However, our second result indicated the similar degrees of MI among all
701 four features, which seems to be consistent with the disentangling coding. If we were able to examine
702 other features, they could exhibit similar degrees of MI, which appears to be consistent with coding
703 disentangling features rather than coding many geometrically definable contour features. We
704 investigated the neural coding from the viewpoint of the formation of object representation. Since
705 classification is another crucial function of the visual system, an investigation from the viewpoint of
706 classification would be interesting and helpful for the further understanding of the intermediate-level
707 cortical representation.

708

709

710

711 **References**

- 712 Arcizet, F., Jouffrais, C., & Girard, P. (2008). Natural textures classification in area V4 of the
713 macaque monkey. *Exp Brain Res*, 189(1), 109-120. [https://doi.org/10.1007/s00221-008-1406-](https://doi.org/10.1007/s00221-008-1406-9)
714 9
- 715 Attneave, F. (1954). Some informational aspects of visual perception. *Psychol Rev*, 61(3), 183-193.
- 716 Bertamini, M., & Wagemans, J. (2013). Processing convexity and concavity along a 2-D contour:
717 figure-ground, structural shape, and attention. *Psychon Bull Rev*, 20(2), 191-207.
718 <https://doi.org/10.3758/s13423-012-0347-2>
- 719 Burge, J., Fowlkes, C. C., & Banks, M. S. (2010). Natural-scene statistics predict how the figure-
720 ground cue of convexity affects human depth perception. *Journal of Neuroscience*, 30(21),
721 7269-7280. <https://doi.org/10.1523/JNEUROSCI.5551-09.2010>
- 722 Carlson, E. T., Rasquinha, R. J., Zhang, K., & Connor, C. E. (2011). A sparse object coding scheme in
723 area V4. *Curr Biol*, 21(4), 288-293. <https://doi.org/10.1016/j.cub.2011.01.013>
- 724 Cover, T. M., & Thomas, J. A. (2006). *Elements of Information Theory*. John Wiley & Sons, Inc.,
725 Hoboken, NJ, U.S.A.
- 726 Dado, T., Papale, P., Lozano, A., Le, L., Wang, F., van Gerven, M., Roelfsema, P., Güçlütürk, Y., &
727 Güçlü, U. (2023). BRAIN2GAN: FEATURE-DISENTANGLED NEURAL CODING OF
728 VISUAL PERCEPTION IN THE PRIMATE BRAIN. *bioRxiv*.
729 <https://doi.org/10.1101/2023.04.26.537962>
- 730 David, S. V., Hayden, B. Y., & Gallant, J. L. (2006). Spectral receptive field properties explain shape
731 selectivity in area V4. *J Neurophysiol*, 96(6), 3492-3505.
732 <https://doi.org/10.1152/jn.00575.2006>
- 733 El-Shamayleh, Y., & Pasupathy, A. (2016). Contour Curvature As an Invariant Code for Objects in
734 Visual Area V4. *Journal of Neuroscience*, 36(20), 5532-5543.
- 735 Elder, J. H., Oleskiw, T. D., & Freund, I. (2018). The role of global cues in the perceptual grouping of
736 natural shapes. *J Vis*, 18(12), 14. <https://doi.org/10.1167/18.12.14>
- 737 Gallant, J. L., Braun, J., & Van Essen, D. C. (1993). Selectivity for polar, hyperboic, and cartesian
738 gratings in Macaque visual cortex. *Science*, 259, 100-103.
- 739 Gerhardstein, P., Tse, J., Dickerson, K., Hipp, D., & Moser, A. (2012). The human visual system uses
740 a global closure mechanism. *Vision Res*, 71, 18-27.
741 <https://doi.org/10.1016/j.visres.2012.08.011>
- 742 Habak, C., Wilkinson, F., Zakher, B., & Wilson, H. R. (2004). Curvature population coding for
743 complex shapes in human vision. *Vision Res*, 44(24), 2815-2823.
744 <https://doi.org/10.1016/j.visres.2004.06.019>
- 745 Hong, H., Yamins, D. L., Majaj, N. J., & DiCarlo, J. J. (2016). Explicit information for category-
746 orthogonal object properties increases along the ventral stream. *Nat Neurosci*, 19(4), 613-622.
747 <https://doi.org/10.1038/nn.4247>
- 748 Kim, T., Bair, W., & Pasupathy, A. (2019). Neural Coding for Shape and Texture in Macaque Area
749 V4. *J Neurosci*, 39(24), 4760-4774. <https://doi.org/10.1523/JNEUROSCI.3073-18.2019>

- 750 Kimura, K., Kodama, A., Yamane, Y., & Sakai, K. (2022). Figure-ground responsive fields of monkey
751 V4 neurons estimated from natural image patches. *PLoS One*, *17*(6).
752 <https://doi.org/10.1371/journal.pone.0268650>
- 753 Klindt, D., Sanborn, S., Acosta, F., Poitevin, F., & Miolane, N. (2023). IDENTIFYING
754 INTERPRETABLE VISUAL FEATURES IN ARTIFICIAL AND BIOLOGICAL NEURAL
755 SYSTEMS. *arXIV*.
- 756 Kodama, A., Kimura, K., & Sakai, K. (2022). Dimensionality of the intermediate-level representation
757 of shape and texture in monkey V4. *Neural Netw*, *153*, 444-449.
758 <https://doi.org/10.1016/j.neunet.2022.06.027>
- 759 Kriegeskorte, N., Mur, M., & Bandettini, P. (2008). Representational similarity analysis - connecting
760 the branches of systems neuroscience. *Front Syst Neurosci*, *2*, 4.
761 <https://doi.org/10.3389/neuro.06.004.2008>
- 762 Kubilius, J., Wagemans, J., & Op de Beeck, H. P. (2014). A conceptual framework of computations in
763 mid-level vision. *Front Comput Neurosci*, *8*, 158. <https://doi.org/10.3389/fncom.2014.00158>
- 764 Mehrani, P., & Tsotsos, J. K. (2023). Learning a Model of Shape Selectivity in V4 Cells Reveals
765 Shape Encoding Mechanisms in the Brain. *J Neurosci*, *43*(22), 4129-4143.
766 <https://doi.org/10.1523/JNEUROSCI.1467-22.2023>
- 767 Okazawa, G., Hatch, C. E., Mancoo, A., Machens, C. K., & Kiani, R. (2021). Representational
768 geometry of perceptual decisions in the monkey parietal cortex. *Cell*, *184*(14), 3748-3761
769 e3718. <https://doi.org/10.1016/j.cell.2021.05.022>
- 770 Okazawa, G., Tajima, S., & Komatsu, H. (2015). Image statistics underlying natural texture selectivity
771 of neurons in macaque V4. *Proc Natl Acad Sci USA*, *112*(4), E351-360.
772 <https://doi.org/10.1073/pnas.1415146112>
- 773 Papale, P., Leo, A., Handjaras, G., Cecchetti, L., Pietrini, P., & Ricciardi, E. (2020). Shape coding in
774 occipito-temporal cortex relies on object silhouette, curvature, and medial axis. *J*
775 *Neurophysiol*, *124*(6), 1560-1570. <https://doi.org/10.1152/jn.00212.2020>
- 776 Pasupathy, A., & Connor, C. E. (1999). Responses to contour features in Macaque area V4. *J*
777 *Neurophysiol*, *82*, 2490-2502.
- 778 Pasupathy, A., & Connor, C. E. (2001). Shape representation in area V4: position-specific tuning for
779 boundary conformation. *J Neurophysiol*, *86*, 2505-2519.
- 780 Pasupathy, A., & Connor, C. E. (2002). Population coding of shape in area V4. *Nat Neurosci*, *5*(12),
781 1332-1338. <https://doi.org/10.1038/nn972>
- 782 Pasupathy, A., Kim, T., & Popovkina, D. V. (2019). Object shape and surface properties are jointly
783 encoded in mid-level ventral visual cortex. *Curr Opin Neurobiol*, *58*, 199-208.
784 <https://doi.org/10.1016/j.conb.2019.09.009>
- 785 Pasupathy, A., Popovkina, D. V., & Kim, T. (2020). Visual Functions of Primate Area V4. *Annu Rev*
786 *Vis Sci*, *6*, 363-385. <https://doi.org/10.1146/annurev-vision-030320-041306>
- 787 Rensink, R. A., & Enns, J. T. (1995). Preemption effects in visual search: evidence for low-level
788 grouping. *Psychol Rev*, *102*(1), 101-130.
- 789 Roe, A. W., Chelazzi, L., Connor, C. E., Conway, B. R., Fujita, I., Gallant, J. L., Lu, H., & Vanduffel,
790 W. (2012). Toward a unified theory of visual area V4. *Neuron*, *74*, 12-29.

- 791 Roelfsema, P. R. (2023). Solving the binding problem: Assemblies form when neurons enhance their
792 firing rate-they don't need to oscillate or synchronize. *Neuron*, *111*(7), 1003-1019.
793 <https://doi.org/10.1016/j.neuron.2023.03.016>
- 794 Rose, O., Johnson, J., Wang, B., & Ponce, C. R. (2021). Visual prototypes in the ventral stream are
795 attuned to complexity and gaze behavior. *Nat Commun*, *12*(1), 6723.
796 <https://doi.org/10.1038/s41467-021-27027-8>
- 797 Sajda, P., & Finkel, L. H. (1995). Intermediate-level visual representations and the construction of
798 surface perception. *Journal of Cognitive Neuroscience*, *7*(2), 267-291.
- 799 Sakai, K., Matsuoka, S., Kurematsu, K., & Hatori, Y. (2015). Perceptual representation and
800 effectiveness of local figure-ground cues in natural contours. *Front Psychol*, *6*, 1685, Article
801 1685. <https://doi.org/10.3389/fpsyg.2015.01685>
- 802 Sakai, K., Sakata, Y., & Kurematsu, K. (2021). Interaction of surface pattern and contour shape in the
803 tilt after effects evoked by symmetry. *Sci Rep*, *11*(1). [https://doi.org/10.1038/s41598-021-](https://doi.org/10.1038/s41598-021-87429-y)
804 [87429-y](https://doi.org/10.1038/s41598-021-87429-y)
- 805 Schmidt, F., & Schmidt, T. (2014). Rapid processing of closure and viewpoint-invariant symmetry:
806 behavioral criteria for feedforward processing. *Psychol Res*, *78*(1), 37-54.
807 <https://doi.org/10.1007/s00426-013-0478-8>
- 808 Schmidtman, G., Jennings, B. J., & Kingdom, F. A. (2015). Shape recognition: convexities,
809 concavities and things in between. *Sci Rep*, *5*, 17142. <https://doi.org/10.1038/srep17142>
- 810 Sharman, R., & Gheorghiu, E. (2018). Spatiotemporal and Luminance Contrast Properties of
811 Symmetry Perception. *Symmetry*, *10*(6). <https://doi.org/10.3390/sym10060220>
- 812 Shishikura, M., Tamura, H., & Sakai, K. (2023). Correlation between neural responses and human
813 perception in figure-ground segregation. *Front Syst Neurosci*, *16*, 999575.
814 <https://doi.org/10.3389/fnsys.2022.999575>
- 815 Timme, N. M., & Lapish, C. (2018). A Tutorial for Information Theory in Neuroscience. *eNeuro*, *5*(3).
816 <https://doi.org/10.1523/ENEURO.0052-18.2018>
- 817 Weiner, K. F., & Ghose, G. M. (2015). Population coding in area V4 during rapid shape detections. *J*
818 *Neurophysiol*, *113*(7), 3021-3034. <https://doi.org/10.1152/jn.01044.2014>
- 819 Willeke, K. F., Restivo, K., Franke, K., Nix, A. F., Cadena, S. A., Shinn, T., Nealley, C., Rodriguez,
820 G., Patel, S., Ecker, A. S., Sinz, F. H., & Tolias, A. S. (2023). Deep learning-driven
821 characterization of single cell tuning in primate visual area V4 unveils topological
822 organization. *bioRxiv*. <https://doi.org/10.1101/2023.05.12.540591>
- 823 Yamane, Y., Carlson, E. T., Bowman, K. C., Wang, Z., & Connor, C. E. (2008). A neural code for
824 three-dimensional object shape in macaque inferotemporal cortex. *Nat Neurosci*, *11*(11),
825 1352-1360. <https://doi.org/10.1038/nn.2202>
- 826 Yamane, Y., Kodama, A., Shishikura, M., Kimura, K., Tamura, H., & Sakai, K. (2020a). *Data*
827 *associated with publication "Population coding of figure and ground in natural image*
828 *patches by V4 neurons."* Osaka University Knowledge Archive
829 <https://doi.org/10.18910/73784>
- 830 Yamane, Y., Kodama, A., Shishikura, M., Kimura, K., Tamura, H., & Sakai, K. (2020b). Population
831 coding of figure and ground in natural image patches by V4 neurons. *PLoS One*, *15*(6),
832 e0235128. <https://doi.org/10.1371/journal.pone.0235128>

833 Zeman, A. A., Ritchie, J. B., Bracci, S., & Op de Beeck, H. (2020). Orthogonal Representations of
834 Object Shape and Category in Deep Convolutional Neural Networks and Human Visual
835 Cortex. *Sci Rep*, 10(1). <https://doi.org/10.1038/s41598-020-59175-0>

836

837

eNeuro Accepted Manuscript

838 **Figure Captions**

839 **Figure 1**

840 (A) Four examples of closure. The yellow dots and ellipses indicate the center and extent of the CRFs,
841 respectively. The closure values were the percentages of the radial lines extending from the CRF
842 center that crossed the contour. The gray dots are the points on the contour. (B) Four examples of
843 curvature. The gray dots are the points on the contour, and the gray regions indicate the figure regions.
844 The small dots and ellipses in black indicate the center and extent of the CRFs. The blue squares
845 indicate the windows for the computation. The pink lines indicate the circles fitted to the contours
846 within the CRF and window. Refer to the main text and Extended Data Figure 1-2 for details. (C) Four
847 examples of symmetry. The gray dots indicate the sampled points on the contour. The red lines are the
848 mid-line of the stimulus used for the computation (vertical in these cases). (D) Four examples of
849 orientation. (Left panels) The red dots and ellipses indicate the center and extent of the CRFs. The
850 gray dots are the points on the contour. (Right panels) The histograms of the local orientations within
851 the CRF. The red lines on the histograms indicate the mean local orientation, which are the orientation
852 values for the combinations of the neuron and stimulus. Example tuning maps for closure (E),
853 curvature (F), symmetry (G), and orientation (H). The asterisks indicate the significance of tuning.
854 The bottom-left schematics illustrate the degree of the feature. (I) Example time courses of ten
855 neurons that showed significant tuning. The original stimuli and their correlation between the closure
856 and curvature values are shown in Extended Data Figure 1-1 and 1-3, respectively.

857

858

859 **Figure 2**

860 (A) Example tuning curves for two neurons computed from the responses to all stimuli including
861 natural and silhouette stimuli. Arrows represent the peaks of the individual tuning curves. (B) The
862 probability distributions of the four contour features of the stimulus set. (C) The distributions of the
863 optimal feature-values of the neurons. The arrows correspond to the peaks in the individual tuning
864 maps shown in (A). (D) The normalized distributions of the optimal feature-values; (C) was
865 normalized by (B).

866

867

868 **Figure 3**

869 (A) The histogram of the number of significant features of individual neurons. The detailed numbers
870 are shown in Extended Data Figure 3-1. (B) The distribution of the normalized tuning strengths of the

871 optimal closure and curvature, with the enlargement in the top-right inset. The blue, red, and green
872 dots indicate the neurons with significant tuning for closure, curvature, and both of them, respectively.
873 (C) The distribution of the cross-tuning between closure and curvature (the combination of optimal
874 closure and curvature) of individual neurons that exhibited significance to closure and/or curvature.
875 The colors represent the number of neurons. (D) The distribution of closure and curvature values
876 across the stimuli. (E) The normalized probability distribution of the cross-tuning; (C) was normalized
877 by (D). The colors represent the probability. (F), (G), and (H) are the same plots as (C), (D), and (E),
878 respectively, for the neurons with significant tuning for both closure and curvature.

879

880

881 Figure 4

882 (A) The top panel shows the histograms for the MI_{clos} . The orange bars indicate the distributions of
883 neurons with significant tuning to closure, and blue bars all neurons. The orange and blue vertical
884 lines indicate the mean MI values for the significant and all neurons, respectively. The bottom panels
885 are example tuning maps of neurons with small, medium, and large MI values (from left to right), with
886 the conventions same as Figure 1E. (B), (C), and (D) show the histograms and example tuning maps
887 for MI_{curv} , MI_{symm} , and MI_{orien} , respectively. (E) The combinations of MI_{clos} , MI_{curv} , MI_{symm} , and MI_{orien}
888 for individual neurons in the order of the sum of the four MIs. The colors indicate the types of MI. (F)
889 The ratios of the greatest MI with respect to the sum of the four MIs. The conventions are the same as
890 (E). The horizontal dotted line indicates the even distribution (0.25). (G) The ratios of the least MI
891 with respect to the sum of the four MIs. The conventions are the same as (F). The analyses including
892 the neurons with a small number of spikes are shown in Extended Data Figure 4-1.

893

894

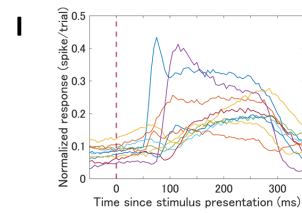
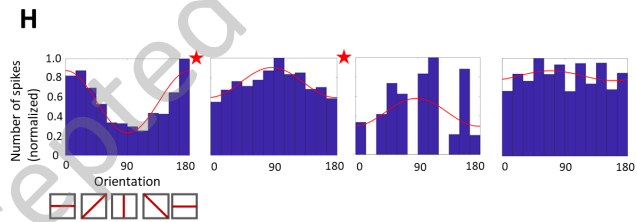
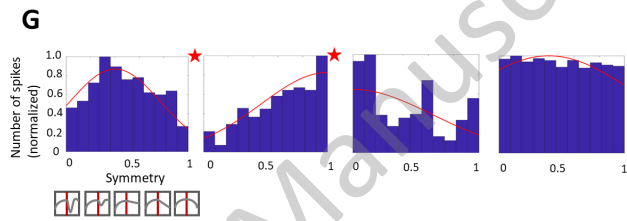
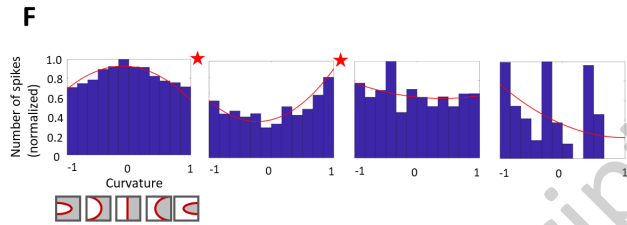
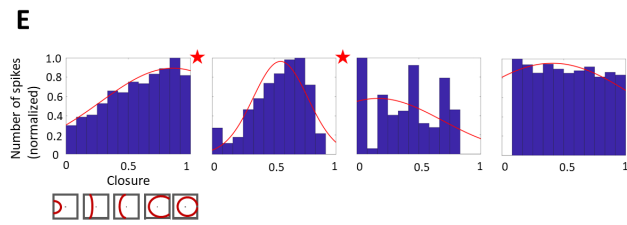
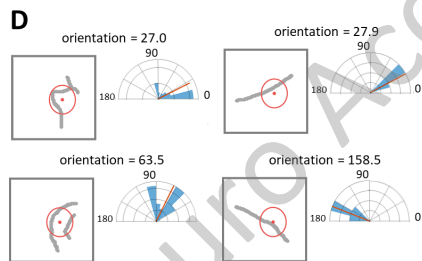
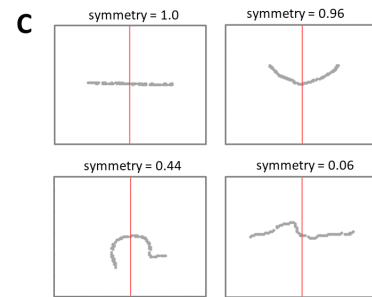
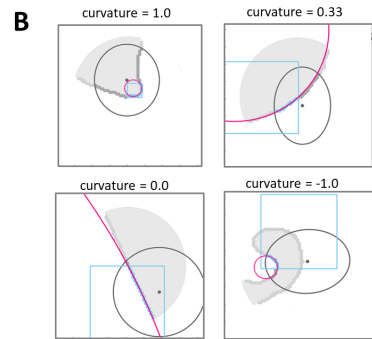
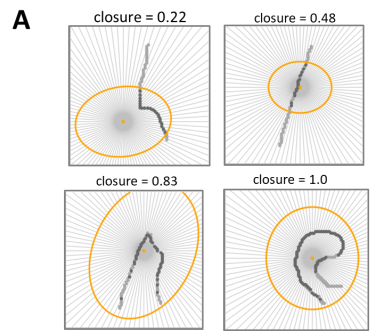
895 Figure 5

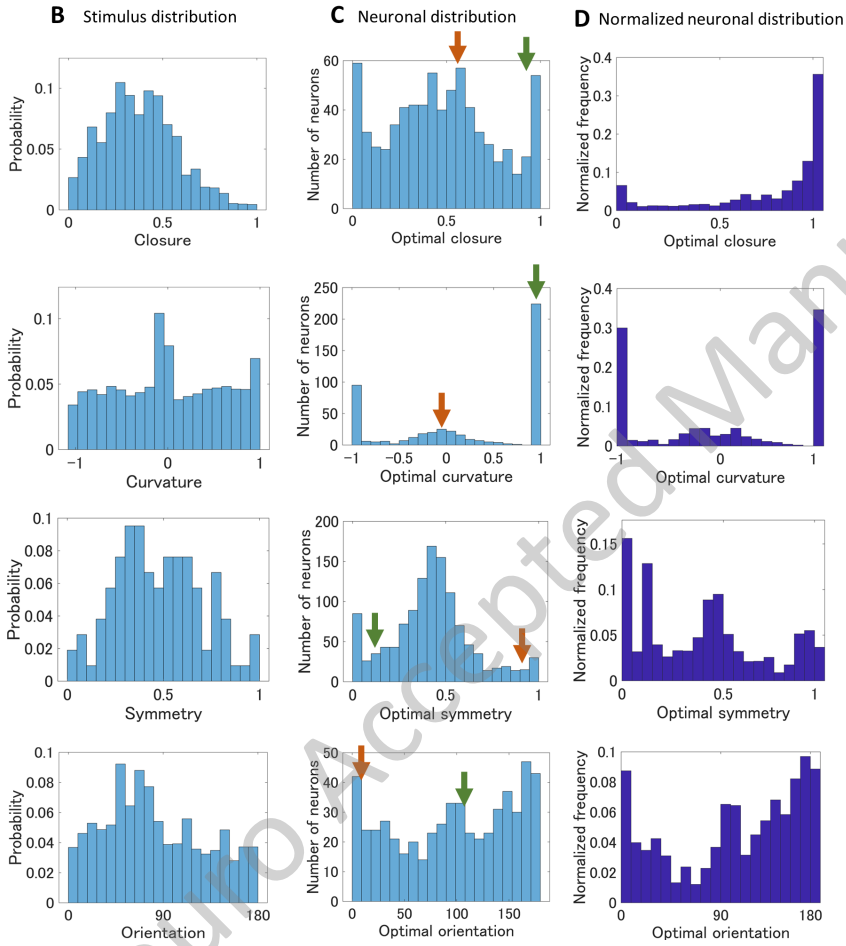
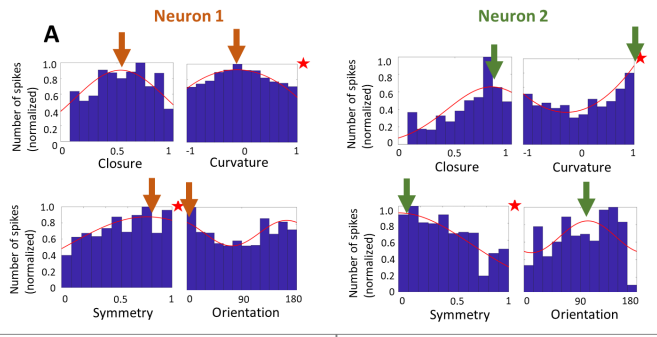
896 (A) The top panel is the two-dimensional MDS map generated from both natural and silhouette
897 stimuli. Refer to Extended Data Figure 5-1 for the stress. The dots represent individual neurons. The
898 neurons are divided horizontally into five groups (as shown in different colors) so as to include the
899 equal number of neurons. Stimuli that evoked the strong responses to example neurons are shown in
900 Extended Data Figure 5-2. The middle panel shows the ratios of neurons with significant tuning with
901 moving average (refer to Methods for details). The blue, orange, yellow, and purple lines show the
902 ratios of significance to closure, curvature, symmetry, and orientation, respectively. The abscissa
903 corresponds to that of the MDS map on the top. The shades represent standard deviation. The bottom

904 panel shows the mean number of significant contour-features along with the primary axis of the MDS
905 map, together with the normalized mean optimal closure and curvature in blue and orange lines,
906 respectively. (B) The MDS map generated from the responses to silhouette stimuli (the top panel), the
907 ratios of the significantly tuned neurons (the middle panel), and the mean number of significant
908 contour-features together with the mean optimal closure and curvature (the bottom panel). The
909 conventions are the same as (A). (C) The left panel is the generated MDS map identical to (A) but
910 with vertical grouping. The right panel represents NS preference (refer to Methods). The ordinate
911 corresponds to that of the MDS map. The blue line indicates the moving mean of the NS preference
912 and the shades represent standard deviation.

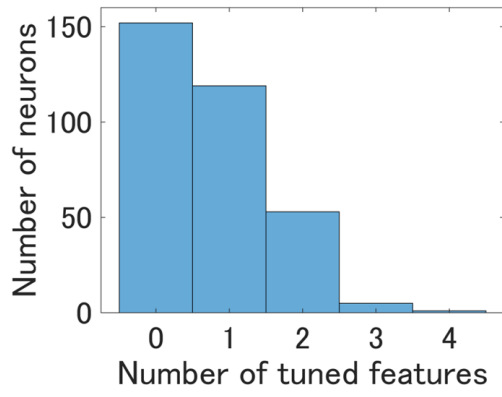
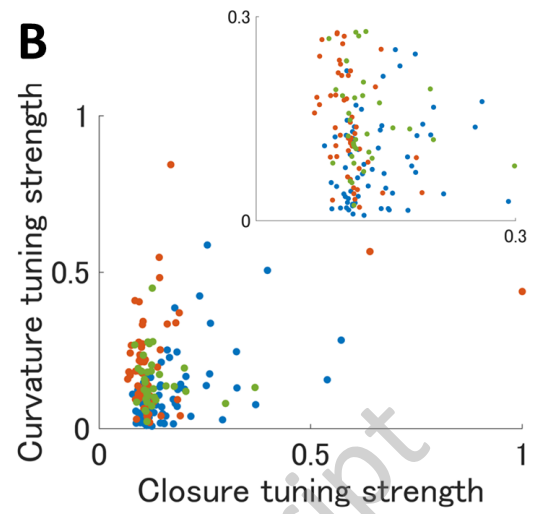
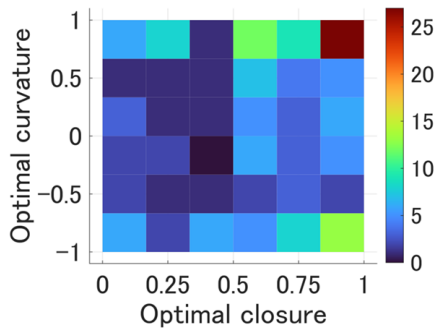
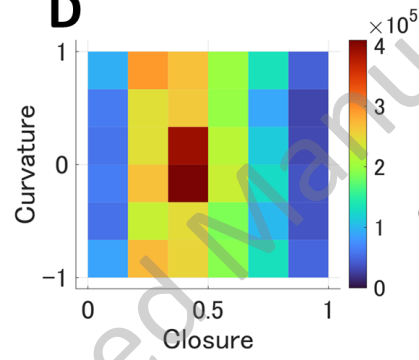
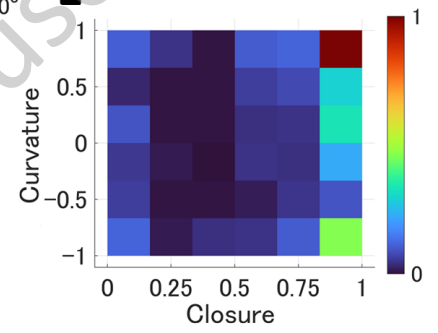
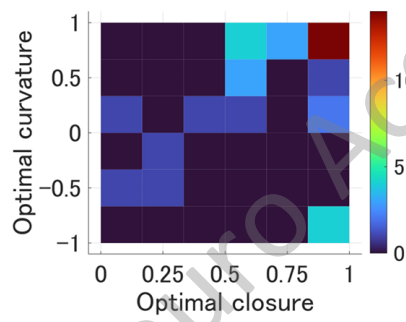
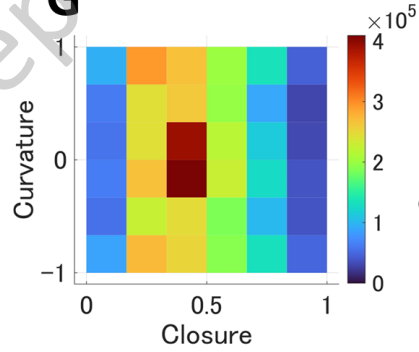
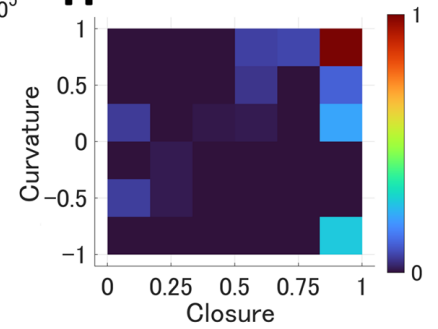
913

eNeuro Accepted Manuscript





eNeuro.org Preprint Manuscript

A**B****C****D****E****F****G****H**

eNeuro Accepted Manuscript

